https://doi.org/10.1016/j.jsv.2020.115653

Vibro-acoustic analysis of parallel barriers integrated with flexible panels

Zhibo Wang[1], Yat Sze Choy[1*] and Chunqi Wang[2]

[1] Department of Mechanical Engineering, The Hong Kong Polytechnic University, Hung Hom, Kowloon, Hong Kong SAR, China

[2] Lab of Aerodynamics and Acoustics, HKU-Zhejiang Institute of Research and Innovation, Lin An, 311305, Zhejiang, China

*Corresponding author email: mmyschoy@polyu.edu.hk

Abstract

In urban communities, parallel barriers are commonly erected for controlling environmental noise such as traffic and construction noise. However, owing to the formation of multiple reflection waves between the parallel barriers, their performance may be worse than that of a single barrier. To improve the performance of parallel barriers, a small piece of flush-mounted panel backed by a slender cavity in an otherwise rigid wall of barriers is proposed. With the excitation of the incident wave from a sound source inside the parallel barriers, the flexible panel vibrates, and sound is radiated out to undergo acoustic interference with the sound field between the parallel barriers. Consequently, the sound energy in this space and diffraction wave at the barrier top edge are reduced over a broad band in the low-frequency regime. A theoretical model for dealing with vibro-acoustic coupling between the open cavity and the vibrating panel in a two-dimensional configuration is established to investigate the sound suppression mechanism in the shadow zone. With optimal structural properties of the panel, an additional averaged insertion loss of approximately 3.95 dB can be achieved at 80–1000 Hz. The theorical results, which are experimentally validated, pave the way for the application of the flexible panel devices (FPDs) for improving the noise reduction of parallel barriers.

Keywords: parallel barriers, flexible panel device, vibro-acoustic analysis

1 Introduction

The mitigation of environmental noise with acoustic barriers is common in highly populated cities. These barriers are installed close to sound sources to reflect and block sound waves, thereby the direct propagation of the sound wave to the receiving zone can be intercepted. To reduce the noise on both roadsides, generally one more barrier is erected along the roadsides to form parallel barriers. However, their performance deteriorates when they are close to each other owing to multiple reflection, which forms a reverberant sound field within the boundaries [1-3]. To deal with this deterioration, absorption layers have been added on the inner surfaces of parallel barriers [4,5]. However, the conventional porous absorptive materials cannot perform well at low frequencies and cause environmental problems such as the accumulation of dust and bacteria. Alternatively, barriers with tilted angles or different edge profiles, (e.g., circular, T-shaped, Y-shaped, arrow, and branched profiles) have been designed, and their performances have been evaluated [4-6]. However, the top edges of the barriers are too bulky for low frequencies. To reduce multiple reflections, Monazzam and Fard suggested the design of a sloped median barrier with different angles to redirect sound waves upwards, thereby diminishing the diffraction at the barrier top and improving the barrier efficiency [7]. In addition, Pan et al. [8] proposed a wave trapping barrier, in which the barrier inner wall is mounted with a series of wedges in the shape of trapezoids or triangular boxes, and Yang et al. [2] investigated the mechanism theoretically. They pointed out that the wedges redirect the reflected waves downward to the ground so that the sound is trapped within the space confined by the two barriers. Moreover, the wedge profile influences the sound pressure redistribution and resonance features, thereby modifying the diffraction strength at the barrier top. Wang et al. [9] introduced the use of the inhomogeneous impedance of an array of hollow narrow tubes of varied depths on barrier wall surfaces. The acoustic trapped modes between the barriers are altered, which improves the noise reduction at the receiver.

Recently, the Helmholtz resonator (HR) was used to reduce the noise radiation from the parallel barriers [10]. The HR was mounted on the inner surface, and significant noise reduction was achieved around the resonator's natural frequency in the shadow zone behind the barriers. However, the noise reduction frequency range of the HR remains narrow although the array of resonators improves the reduction of multiple peak frequencies.

To widen the working frequency range, this paper proposes to mount the inner surfaces of the parallel barriers with a flexible panel device (FPD) which is composed of a flexible panel and a compact backing cavity. The configuration of the FPD is similar to the panel silencer which was proposed by Huang [11] to attenuate the duct noise. To simplify the practical implementation, Wang et al. [12] replaced the simply supported boundary condition of the panel by the clamped-clamped one. The transmission loss was attractive from low to medium frequency range [13]. To further broaden the noise reduction band, the micro-perforations was introduced for the flexible panel by Wang et al. [14] and Xi et al.[15]. The purpose of such a flexible micro-perforated panel was to compensate for the deficiency in the pass-band caused by the insufficient sound reflection due to the panel by absorbing sound through micro-perforations. Besides above studies, the use of flexible panel to influence the sound field inside or outside cavity has been found in many literatures [16-20]. For instance, Dowell and Voss [16] investigated a cavity-backed panel, and Pretlove [17] derived an expression for cavity-backed panels vibration using in-vacuum modes. Guy [18], Pan and Bies [19], and Tanaka et. al [20] investigated the influence of the flexible panel on the sound field of a confined cavity. Moreover, some researchers studied the structural–acoustic coupling between the sound field in a semi-infinite space and a baffled opened cavity covered partially by a flexible structure [21-23]. These studies provide useful insight into the structural–acoustic interaction and acoustic coupling of baffled open cavities. However, very little attention has been devoted to the noise control of open cavities formed by parallel barriers with flexible panel. Moreover, the mechanism of sound suppression in the open cavity system is different from that of a panel silencer in the duct. In this study, the flexible panel vibrates due to the incident sound and sound wave is subsequently radiated out to undergo acoustic interference with the original sound waves confined by the parallel barriers. This leads to the distortion of the sound field between the parallel barriers. With a proper design of the FPD, the sound intensity at the barrier top edge decreases, which improves the noise reduction in the shadow zone.

To analyze the performance of parallel barriers, diffraction theories [24, 25] are conventionally used to predict the wave propagation into the shadow zone. However, these analytical methods are not capable of dealing with barriers with complex profiles, neither with the vibro-acoustic coupling and sound interference between the sound waves in the open cavity and the sound waves radiated from the vibrating panel of the FPD. For these cases, the finite element method (FEM) [2, 9] or the boundary element method (BEM) [26, 27] are a good option. In addition, a hybrid BEM–FEM coupling approach has been developed to study the acoustic performance when the acoustic barriers are considered acoustically elastic walls [28]. However, these numerical methods are insufficient in revealing the sound abatement mechanisms. Recently, the non-Hermitian Hamilton principle [29-31], which also called technically coupled mode theory, was applied by Tong et al.[32] and Wang et al.[10] to predict the acoustic performance of parallel barriers. In this method, the acoustic space of the parallel barriers is decoupled into two subspaces: a confined cavity space and a semi-infinite space. The sound field of the parallel barriers is represented by the coupled modal variables corresponding to these two sub-domains. In this study, the non-Hermitian Hamilton principle is adopted and further extended to deal with the vibro-acoustic coupling in acoustical open space.

The objectives of this study are: (1) establishing a theoretical model that is capable of dealing with the vibro-acoustic behavior between the open cavity and vibrating panel; (2) conducting a systematic analysis of the structural-acoustic interaction of the parallel barriers with the flexible panel and backing cavity. (3) revealing the control mechanism of the acoustic modal response in the open cavity by means of the FPD and investigating its impact on the sound suppression performance.

2 Theoretical model for structural-acoustic interaction

In this section, a theoretical model is presented that includes the structural-acoustic interaction and acoustic interference between the confined cavity space and semi-infinite open space.

2.1 Descriptions of the coupling system

Fig. 1 illustrates a model of two identical barriers erected on the ground, with the assumption of unchanged cross-section in the *z*-direction. A Cartesian coordinate system is adopted where the origin is fixed at the upper left corner of the barriers. The two parallel barriers have a height of L_y and horizontal distance of L_x. A harmonic sound field is excited by a point source located at $\boldsymbol{x_s} = (x_s, y_s)$. On the barrier walls facing the noise source is lined by multiple flexible panel devices (FPDs). The i-th panel has a length of $L_{p,i}$ and is backed by a rectangular rigid-walled cavity of depth $D_{cav,i}$ and length $L_{cav,i}$. The lower end of the panel has a distance of $H_{p,i}$ from the ground. The entire space of the parallel barriers with the open region is divided into the cavity space Ω_a and upper-half semi-infinite space Ω_b. The cavity space Ω_a is also called the barrier space and the semi-infinite space Ω_b is the outside space. These two acoustic domains are connected through the cavity opening with area s_{op}. Our interest here is the acoustic interaction among the barrier space Ω_a, the outside space Ω_b and FPDs.

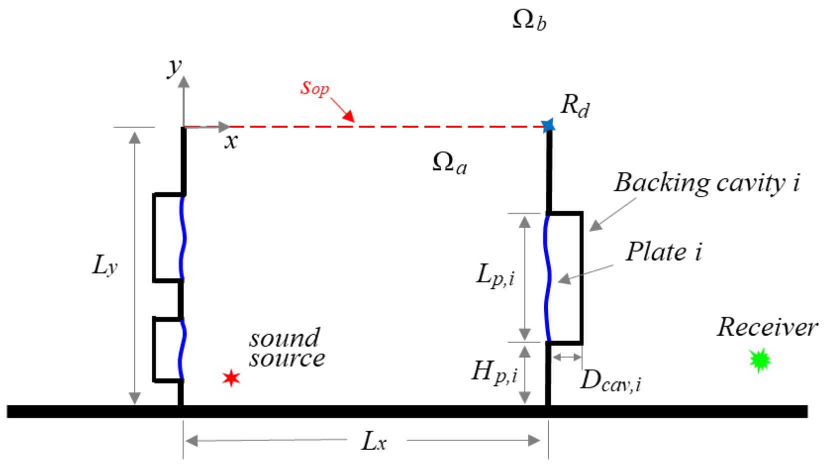

Fig. 1. Sketch of the parallel barriers with multiple flexible panel devices (FPDs).

Omitting the time harmonic dependence, the governing equations for the acoustic fields in barrier space Ω_a, the outside space Ω_b and backing cavity of the panel, are respectively expressed as

$$\nabla^2 p_a(\boldsymbol{x}) + k^2 p_a(\boldsymbol{x}) = -Q_s \delta(\boldsymbol{x} - \boldsymbol{x}_s), \tag{1}$$

$$\nabla^2 p_b(\boldsymbol{x}) + k^2 p_b(\boldsymbol{x}) = 0, \tag{2}$$

$$\nabla^2 p_{cav,i}\ \ \boldsymbol{x}\ + k^2 p_{cav,i}\ \ \boldsymbol{x}\ = 0\,, \tag{3}$$

where $k = \omega/c_0$ is the wavenumber, c_0 is the speed of sound, and Q_s is the source strength. p_a, p_b and $p_{cav,i}$ indicate the sound pressure in space Ω_a, Ω_a and i-th backing cavity, respectively.

With the constant bending stiffness and density along the uniform panel which is placed vertically, the forced vibration of the panel is governed by [33]

$$\nabla^4 \eta_{p,i}(\boldsymbol{x}') - \gamma\nabla\left[(1-\boldsymbol{x}')\nabla\eta_{p,i}(\boldsymbol{x}')\right] - \Lambda\eta_{p,i}(\boldsymbol{x}') = p_{cav,i} - p_a \tag{4}$$

where $\eta_{p,i}$ is the vibration displacement of the i-th panel at its local coordinate $\boldsymbol{x}'$; γ and Λ are the parameters related to the structural property of the panel.

According to the momentum equilibrium at the opening s_{op}, we have

$$\left.\frac{\partial p_a}{\partial n}\right|_{s_{op}} = -i\rho\omega v_o\,, \tag{5}$$

where, v_o is the particle velocity at the opening whose normal direction is outward.

On the panel surface facing the barrier space, the velocity continuity condition must be satisfied as

$$\left.\frac{\partial p_a}{\partial n}\right|_{s_{p,i}} = -i\rho\omega v_{p,i}\,, \tag{6}$$

where $v_{p,i} = i\omega\eta_{p,i}$ is the panel normal vibration velocity.

2.2 Sound field of parallel barriers

The acoustic field within the barrier space Ω_a is expanded as the superposition of the closed-cavity modal functions, which have a complete and orthogonal feature:

$$p_a(\boldsymbol{x}) = \sum_{j=1}^{N} a_j \phi_j(\boldsymbol{x})\,, \tag{7}$$

where a_j is the modal response of the j-th closed-cavity mode $\phi_j(\boldsymbol{x})$ and N the maximal number of truncated mode series. For the rectangular barrier space Ω_a in this study, $\phi_j(\boldsymbol{x})$ is calculated as follows:

$$\phi_j\left(\boldsymbol{x}\right)=\psi_{j_x}\left(x\right)\cdot\psi_{j_y}\left(y\right), \tag{8}$$

where $\psi_{j_x}=\sqrt{\left(2-\delta_{0,j_x}\right)/L_x}\cos\left(j_x\pi x/L_x\right)$ and $\psi_{j_y}=\sqrt{\left(2-\delta_{0,j_y}\right)/L_y}\cos\left(j_y\pi y/L_y\right)$ are the components of the j-th mode in x and y directions, respectively, and $\delta_{i,j}$ is the Kronecker delta function.

The normal particle velocity at the opening, v_o, is expressed as a combination of vibration modes:

$$v_o=\sum_{m=1}^{M}b_m\psi_m\left(\boldsymbol{x}\right), \tag{9}$$

where, b_m is the coefficient of $\psi_m(\boldsymbol{x})$ and M the truncated mode number.

Similarly, the sound field in the outside space, Ω_b, is expressed as a function of the normal velocity at the opening surface and Green's function $G_u\left(\boldsymbol{x},\boldsymbol{x}_{op}\right)$ for the upper half space, which is derived from the Kirchhoff-Helmholtz integral equation [10, 32],

$$p_b\left(\boldsymbol{x}\right)=i\rho\omega\int_{s_{op}}G_u\left(\boldsymbol{x},\boldsymbol{x}_{op}\right)v_o ds_{op}\ . \tag{10}$$

By substituting Eq.(9) into Eq.(10), the sound pressure in the outside space Ω_b can be rewritten as follows:

$$p_b\left(\boldsymbol{x}\right)=\sum_{m=1}^{M}b_m\varphi_m\left(\boldsymbol{x}\right), \tag{11}$$

in which

$$\varphi_m\left(\boldsymbol{x}\right)=i\rho\omega\int_{s_{op}}G_u\left(\boldsymbol{x},\boldsymbol{x}_{op}\right)\psi_m\left(\boldsymbol{x}_{op}\right)ds_{op}\ . \tag{12}$$

The parallel barrier is considered an unbaffled open cavity which is formed by placing two thin rigid walls on an infinite rigid surface. Therefore, the Green's function used here is assumed to satisfy the Neumann condition over the unbaffled plane, including the ground, outside surfaces of the barriers, and cavity opening. However, the unbaffled Green's function, $\boldsymbol{G}_u(\boldsymbol{x}, \boldsymbol{x}_{op})$, cannot be expressed analytically and determined numerically. To deal with this, FEM is applied to obtain $\varphi_m(\boldsymbol{x})$ instead of determining $\boldsymbol{G}_u(\boldsymbol{x}, \boldsymbol{x}_{op})$. The procedure is descibribed in Ref. [10] and will not be discussed here.

The sound fields in the cavity space and outside space are coupled based on the continuity condition at the interface $p_a(\boldsymbol{x})\big|_{s_{op}} = p_b(\boldsymbol{x})\big|_{s_{op}}$, such that

$$\sum_{j=1}^{N} a_j \phi_j(\boldsymbol{x}) = \sum_{m=1}^{M} b_m \varphi_m(\boldsymbol{x}). \tag{13}$$

Multiplying $\psi_{jx'}(x')$ at both sides of Eq.(13) and integrating over the opening leads to:

$$\sum_{j=1}^{N} a_j \delta_{j_x, j_x'} \psi_{j_y}(0) = \sum_{m=1}^{M} b_m \int_{s_{op}} \psi_{j_x} \varphi_m ds_{op} . \tag{14}$$

By defining $Z_{j_x,m} = \int_{s_{op}} \psi_{j_x}(\boldsymbol{x}')\varphi_m(\boldsymbol{x}) ds_{op}'$, Eq.(14) can be rewritten as follows:

$$\sum_{j=1}^{N} a_j \delta_{j_x, j_x'} \psi_{j_y}(0) = \sum_{m=1}^{M} b_m Z_{j_x',m} . \tag{15}$$

2.3 Modal dynamics of structural-acoustic interaction

To facilitate the analysis, only the configuration of the parallel barriers with a single FPD mounted on the left wall is considered. Under harmonic vibrations, the panel normal vibration velocity is $v_p = i\omega\eta_p$. By introducing the local coordinate $\xi = (y - H_p)/L_p$, Eq. (4) becomes the following expression:

$$B_p \frac{d^4 v_p}{d\xi^4} - m_p \frac{d}{d\xi}\left[(1-\xi)\frac{dv_p}{d\xi}\right] - \frac{v_p}{i\omega} = p_{cav} - p_a, \tag{16}$$

where $B_p = E_p d_p^3/[12(1-\sigma_p^2)]$ is the bending stiffness, and E_p, σ_p and d_p are the Young's modulus, Poisson's ratio, and thickness of the panel respectively [11]. m_p is the mass per unit surface area of the panel. The damping effect is neglected in theoretical studies since the sound reflection at the panel is dominant [12].

Eq.(16) is a fourth-order linear differential equation with a variable coefficient, resulting in the difficulty in analytically determining the modal functions. Alternatively, Galerkin's method is used to obtain the modal functions of such a uniform beam with clamp-clamped supported at two ends. The detailed procedure is shown in Appendix A. Hence, the panel normal vibration velocity v_p is expanded as the superposition of mode $\hbar_\mu(\xi)$ with amplitude of $V_{p,\mu}$:

$$v_p(y) = \sum_{\mu=1}^{\mu} V_{p,\mu}\hbar_\mu(\xi), \tag{17}$$

in which $\hbar(\xi) = \sum_{t=1}^{T} c_t \vartheta_t(\xi)$, $\vartheta_t(\xi)$ is the modal shape function for the clamped-clamped panel and c_t the corresponsing coefficient. They can be calculated with Eqs.(A.4) -(A.11) in Appendix A.

By substituting Eq.(17) into Eq.(16) and integrating over the panel, Eq.(16) can be transformed as follows:

$$L_\mu V_{p,\mu} = \int_0^1 \hbar_\mu(\xi) p_{cav} d\xi - \int_0^1 \hbar_\mu(\xi) p_a d\xi, \tag{18}$$

where L_μ is the structural operator:

$$L_\mu = \frac{B_p}{i\omega}\left(\frac{\lambda_\mu}{L_p}\right)^4 + m_p i\omega, \tag{19}$$

where λ_μ is the eigenvalue calculated with Eq.(A.8).

The acoustic pressure inside the two-dimensional rectangular backing cavity can be expressed in terms of acoustic modes of rigid-walled cavity neglecting the damping [12, 14, 34]

$$p_{cav}(\boldsymbol{x}) = \sum_t \frac{i\omega\phi_{cav,t}(\boldsymbol{x})}{k^2 - (k_{cav,t})^2}\int_0^1 \left[v_p(y')\phi_{cav,t}(0,y')\right] d\xi', \tag{20}$$

where $v_p(\xi)$ is the normal velocity over the flexible panel, $\phi_{cav,t}$ the *t-th* acoustic mode for the backing cavity, and $k_{cav,t}$ the acoustic wavenumber.

By substituting Eq.(17) into Eq.(20), the sound pressure inside the backing cavity can be rewritten as follows:

$$p_{cav}(\boldsymbol{x}) = \sum_{\nu=1}^{\mu} V_{p,\nu}\, p_{cav,\nu}(\boldsymbol{x}), \tag{21}$$

where $p_{cav,\nu}(\boldsymbol{x})$ is the sound pressure inside the backing cavity caused by the ν-th modal vibration of the unit amplitude:

$$p_{cav,\nu}(\boldsymbol{x}) = \sum_{t=1}^{\boldsymbol{T}} \frac{i\omega\phi_{cav,t}(\boldsymbol{x})}{k^2 - (k_{cav,t})^2}\int_0^1 \hbar_\nu(\xi')\phi_{cav,t}(0,y')\, d\xi'. \tag{22}$$

The cavity impedance, $Z_{cav,\mu\nu}$, is presented as follows:

$$Z_{cav,\mu\nu} = \int_0^1 \hbar_\mu(\xi)\, p_{cav,\nu}(\boldsymbol{x})\, d\xi = \sum_t \frac{i\omega\left(2-\delta_{0,t_x}\right)\left(2-\delta_{0,t_y}\right)}{D_{cav}\left(k^2 - k_{cav,t}^2\right)} I_{t,\mu\nu}\ , \tag{23}$$

where $I_{t,\mu\nu}$ is defined as follows:

$$I_{t,\mu\nu} = \int_0^1 \hbar_\mu(\xi)\phi_{cav,t}(\boldsymbol{x})\int_0^1 \hbar_\mu(\xi')\phi_{cav,t}(\boldsymbol{x})\, d\xi\, d\xi'. \tag{24}$$

Therefore, the first integration on the right side of Eq.(18) can be rewritten with the cavity impedance and modal coefficient of the panel vibration:

$$\int_0^1 \hbar_\mu p_{cav} d\xi = \sum_{\nu=1}^{\mu} V_{p,\nu} Z_{cav,\mu\nu} . \tag{25}$$

The second integration on the right side of Eq.(18) relates the panel vibration to the sound pressure inside the space Ω_a.

$$\int_0^1 \hbar_\mu \left(\xi\right) p_a d\xi = \sum_j a_j Z_{a,j\mu} , \tag{26}$$

where $Z_{a,\mu j} = \int_0^1 \hbar_\mu \left(\xi\right) \phi_j \left(0, y\right) d\xi$.

Substituting Eqs.(25) and (26) into Eq.(18) yields the second set of linear equations for the modal coefficients V_p and a_j:

$$L_\mu V_{p,\mu} = \sum_\nu V_{p,\nu} Z_{cav,\mu\nu} - \sum_j a_j Z_{a,\mu j} . \tag{27}$$

Finally, by applying the second Green identity to the barrier space Ω_a, the following expression can be obtained:

$$a_j \left(k^2 - k_j^2\right) - i\rho\omega \int_{s_{op}} \phi_j v_o ds_{op} - i\rho\omega \int_{s_p} \phi_j v_p ds_p = -i\rho\omega q_s \phi_j \left(\boldsymbol{x}_s\right). \tag{28}$$

Substituting the modal expressions for v_o and v_p into Eq.(28) yields:

$$\begin{aligned} & a_j \left(k^2 - k_j^2\right) - i\rho\omega \sum_m b_m \int_{s_{op}} \phi_j \psi_m ds_{op} \\ & - i\rho\omega \sum_\mu V_{p,\mu} \int_{s_p} \phi_j \hbar_\mu ds_p = -i\rho\omega q_s \phi_j \left(\boldsymbol{x}_s\right) \end{aligned} . \tag{29}$$

With $h_{j\mu} = \int_{s_p} \phi_j \hbar_\mu ds_p$ and the orthogonal property of the eigenmodes, Eq.(29) can be rewritten as follows:

$$a_i \left(k^2 - k_i^2\right) - i\rho\omega \sum_m b_m \psi_{i_y} \left(0\right) \delta_{i_x, m} - i\rho\omega \sum_\mu V_{p,\mu} h_{i,\mu} = -i\rho\omega q_s \phi_i \left(\boldsymbol{x}_s\right). \tag{30}$$

When setting

$$\begin{aligned}\mathbf{A} &= \{a_1,\ a_2,\ \cdots\ ,a_N\}^T; \\ \mathbf{B} &= \{b_1,\ b_2,\ \cdots\ ,b_M\}^T; \\ \mathbf{V_p} &= \{V_{p,1},\ V_{p,2},\ \cdots\ ,V_{p,U}\}^T\end{aligned}\quad , \tag{31}$$

Eqs.(15), (27) and (30) can be expressed as follows:

$$\mathbf{\Phi A}=\mathbf{ZB}, \tag{32}$$

$$\mathbf{LV_p} = \mathbf{Z_{cav}V_p} + \mathbf{Z_a A}, \tag{33}$$

$$\mathbf{A} + \mathbf{MB} + \mathbf{HV_p} = \mathbf{S}. \tag{34}$$

The details about each element in Eqs.(32)-(34) are presented in Appendix B.

The modal coefficients **A**, **B** and $\mathbf{V_p}$ can be solved via inversion of the matrix. With the theoretical model above, the sound field in and outside the parallel barrier integrated with the FPD can be calculated.

3 Performance determination of parallel barriers with FPD

3.1 Model validation

The theoretical method is verified by comparing the calculated results with those obtained from the commercial finite element solver, COMSOL Multiphysics. The parallel barriers have a size of L_x = 1.83 m, L_y = 1 m, and the thickness of the barrier wall is 0.1 m, which are similar to the configurations studied in Refs. [2, 9]. A point source is located at (0.1, -0.9) m, with the source strength q_s = 0.0001 kg s^{-2}. The performance of the FPD depends on the panel property, backing cavity geometry and mounting location. The effects of these parameters will be discussed in the next section. Here, the mass, bending stiffness and length of the panel is m_p = 0.064 kg m^{-1}, B_p = 0.024 N m^{-1} and L_p = 0.4 m, respectively. The cavity is L_{cav} = 0.4 m and D_{cav} = 0.1 m in length and depth, and is located at a height of H_p = 0.1 m. In the theoretical calculation, the modes are truncated to the finite numbers. For the acoustic cavity modes $\phi_j(\boldsymbol{x})$ used in Eq.(7), the total number was N = 300 while those of $\psi_m(\boldsymbol{x})$ in Eq.(9) and $\hbar_\mu(\xi)$ in Eq.(17) were M = 40 and $\boldsymbol{\mu}$ = 40, respectively. The calculated results indicate the mode numbers are sufficient, as a further increase in the number does not make a significant deviation. The sound pressure level (SPL) in the shadow zone of parallel barriers with or without any acoustic treatment has similar variation and pattern [10]. Therefore, the receiving point R1 at (5, -0.9) m is chosen as the typical observation point.

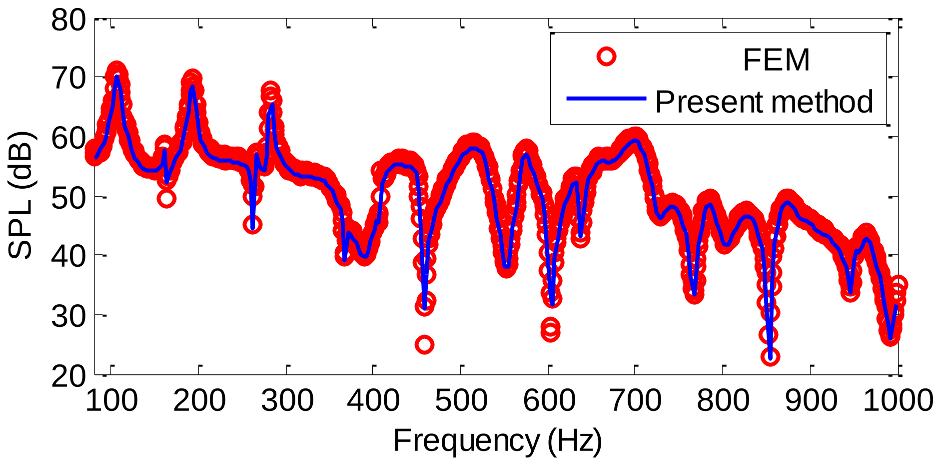

Fig. 2. Comparison of SPL at R1 between the present method and FEM.

Fig. 2 compares the SPL results obtained by the proposed theoretical method and FEM at receiver R1, which is represented by the solid line and open circles, respectively. It reveals that the results obtained by the proposed theory agree well with those by the FEM, which fully support the accuracy of the model established.

3.2 Performance analysis

The performance of the FPD with relatively short length L_p = 0.1 m, namely FPD_1 is discussed in this section. The detailed configuration is listed in Table 1.

Table 1, flexible panel and rectangular backing cavity parameters.

	Flexible plate				Rectangular backing cavity	
	m_p (kg m^{-1})	B_p (N m^{-1})	L_p (m)	H_p (m)	D_{cav} (m)	L_{cav} (m)
FPD$_1$	2	1.2	0.1	0.1	0.1	0.1
FPD$_2$	0.4	0.34	0.4	0.1	0.1	0.4

Fig. 3 compares the SPL spectra at receiver R1 for the parallel barriers without acoustic treatment, with an FPD$_1$ and with a single HR. The natural frequency of the resonator is 281 Hz and is therefore named HR281. The physical diameter of the resonator body branch is 200 mm; the other parameters can be found in Ref. [10]. As shown by the solid blue line in Fig. 3, for the parallel barriers without any acoustic treatment, multiple sharp SPL peaks occur at 109, 198 , 289, 381, 474, 567, 660, 753 and 940 Hz. These frequencies are closely related to the resonances of the barrier space Ω_a. In addition, the sound distributions within the barrier space at these frequencies are similar to their corresponding modal shapes of the enclosed cavity [10]. When the FPD$_1$ is mounted on the left wall of the parallel barriers, the SPL at 289 Hz is reduced from 69.9 dB to 45.0 dB. Moreover, an averaged noise reduction of 5 dB is achieved at frequencies around 289 Hz with a bandwidth of 20 Hz. This frequency corresponds to the first resonance frequency of the panel with a length of 0.1 m. With the use of resonator HR281, a broader noise suppression bandwidth can be achieved. However, the performance is more deteriorated at high frequencies. In view of the overall performance at 80 – 1000 Hz, FPD$_1$ is slightly better than HR281. To widen the frequency range of noise suppression, a longer panel is proposed. The new FPD with a length of L_p = 0.4 m is named FPD$_2$, its structural and geometrical parameters are listed in Table 1.

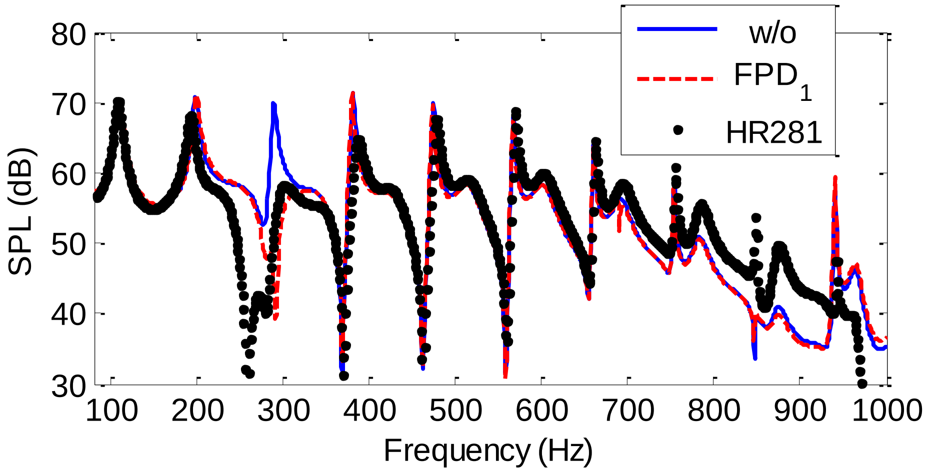

Fig. 3. SPL comparison of parallel barriers integrated with FPD_1 (m_p = 2 kg m^{-1}, B_p = 1.2 N m^{-1} and L_p = 0.1 m) and HR281.

To facilitate the analysis, Table 2 lists the acoustic modes used in Eq. (7), major SPL peak frequencies attributed to the parallel barriers at the receiving point R1, and in-vacuum vibration modes of the panel in FPD_1 and FPD_2. The SPL peaks at the receiver are closely related to the resonances of the enclosure and the panel vibration plays an important role. As illustrated in Fig. 3, the third SPL peak can be notably reduced when the FPD_1 with the first resonance frequency of the panel at 251.8Hz is adopted. This is attributed to the dominant first modal response of the in-vacuum panel of FPD_1, which causes the radiated sound to undergo acoustic coupling with the original sound field inside parallel barriers around peak frequency of 289Hz. By contrast, the eighth SPL peak cannot be reduced although its frequency is close to the second resonance of the panel. This is because the radiation effectiveness of the in-vacuum second mode of the short panel is too low for interactions with the sound waves inside the parallel barriers.

Table 2, comparison of the enclosed-cavity resonances, SPL peak frequencies and the in-vacuo resonances of flexile panel in FPDs.

Enclosed-cavity mode		Parallel barriers		in-vacuum modes of the panel in FPD_1		in- vacuum modes of the panel in FPD_2	
Modal indices	Frequency	SPL Peaks	Frequency	Modal indices	Frequency	Modal indices	Frequency
(1,0)	93.7	1	109			3	110.9
(2,0)	187.4	2	198			4	183.3
(3,0)	281.2	3	289	1	251.8	5	273.8
(4,0)	374.9	4	381			6	382.4
(5,0)	468.6	5	474				
(6,0)	562.3	6	567			7	509.1
(7,0)	656	7	660			8	654
(8,0)	749.7	8	753	2	694.1		
(9,0)	843.4					9	816.9
(10,0)	937.2	9	940			10	998

Fig. 4 compares the SPL spectra of the parallel barriers without any acoustic treatment (solid line), with an FPD_2 (dashed line), and two resonators working at two different target frequencies (dotted). One of the resonators is HR281. The other resonator has a natural frequency of 468 Hz; its neck branch length is 10 mm, body branch length is 83 mm, neck branch diameter is 20 mm, and body branch diameter is 90 mm. When these two resonators are mounted on the wall of the parallel barriers, most SPL peaks are reduced significantly, except that at 109 Hz. The SPL peaks at 289, 381, and 474 Hz are reduced by 12.4, 3.4 and 19.8 dB, respectively and the noise is reduced by 2.6 dB on average at 195 – 482 Hz. When the FPD_2 is used, the noise reductions at 289, 381, and 474 Hz are approximately 27.3, 24.6, and 11. 9 dB, respectively. An average noise reduction of 7.8 dB is obtained at 164 – 440 Hz, which results in a wider stopband than two HRs. Thus, the FPD achieves a higher noise reduction at the original sound peaks and wider working frequency band. Consequently, a single FPD outperforms two simultaneously working HRs.

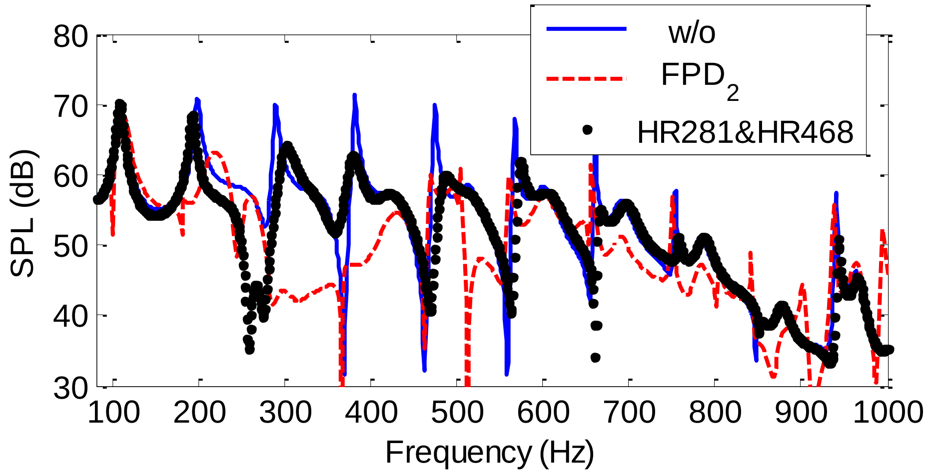

Fig. 4. SPL comparison of parallel barriers integrated with FPD_2 (m_p = 0.4 kg m^{-1}, B_p = 0.34 N m^{-1} and L_p = 0.4 m) and two HRs.

The previously mentioned analysis of the FPD performance focuses on the sound reduction at one receiving point outside the barrier. To study the change in the sound field distribution inside and outside the parallel barriers, the sound map is calculated and shown in Fig. 5. The first and second columns display the SPL distribution of the parallel barriers without and with FPD_2 at 289, 381 and 474 Hz, respectively. These three frequencies correspond to the SPL peaks when the parallel barrier walls are acoustically rigid. With the use of the FPD_2, the sound field inside the barrier space is distorted, and the corresponding SPL at the barrier edges are suppressed. According to the diffraction theory [24, 25], as the incident sound amplitude is suppressed while the incident angle is slightly changed, the SPL behind the barriers are reduced. Moreover, the noise reductions at the two sides of the parallel barriers by the FPD_2 are not identical. The noise reduction in the left-hand zone of the barriers is more significant than that in the right-hand zone of the barriers at 289 and 381 Hz owing to the asymmetric location of the noise control device. However, the noise reductions are almost the same in both sides of the barriers at 474 Hz.

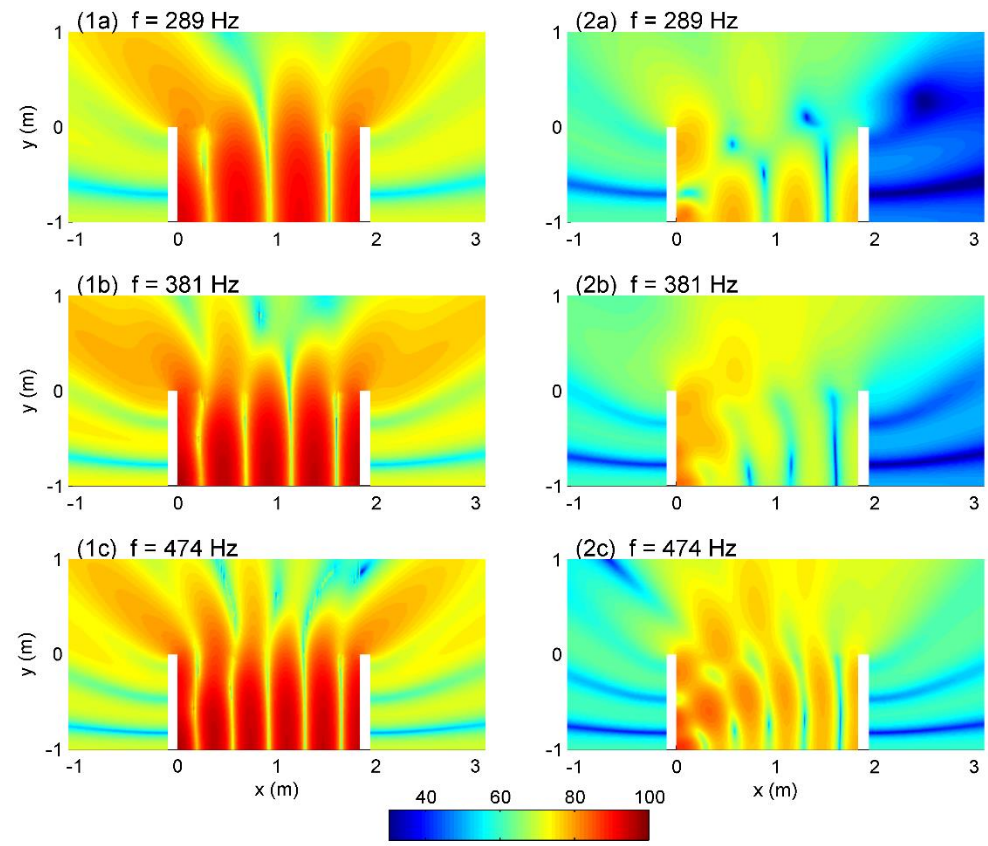

Fig. 5. The SPL field for the parallel barriers with and without FPD_2. (1a), (1b) and (1c) without FPD_2 at f = 289, 381 and 474 Hz; (2a), (2b) and (2c) with FPD_2 at f = 289, 381 and 474 Hz, respectively.

3.3 Mechanism of noise reduction improvement by FPD

3.3.1 Panel modal response

To investigate the noise reduction mechanism by FPD, the modal responses of the cavity mode $\phi_j(\boldsymbol{x})$, external mode $\varphi_m(\boldsymbol{x})$, and panel mode $\hbar(\boldsymbol{x})$ are presented. Fig. 6 illustrates the modal coefficients $|a_j|$, $|b_m|$, and $|V_{p,\mu}|$ for parallel barriers without and with FPD_2 at (0, -0.9) m. The first column of Fig. 6 depicts the modal amplitudes for the cavity, external and panel modes at 289 Hz, while the second column shows those at 474 Hz.

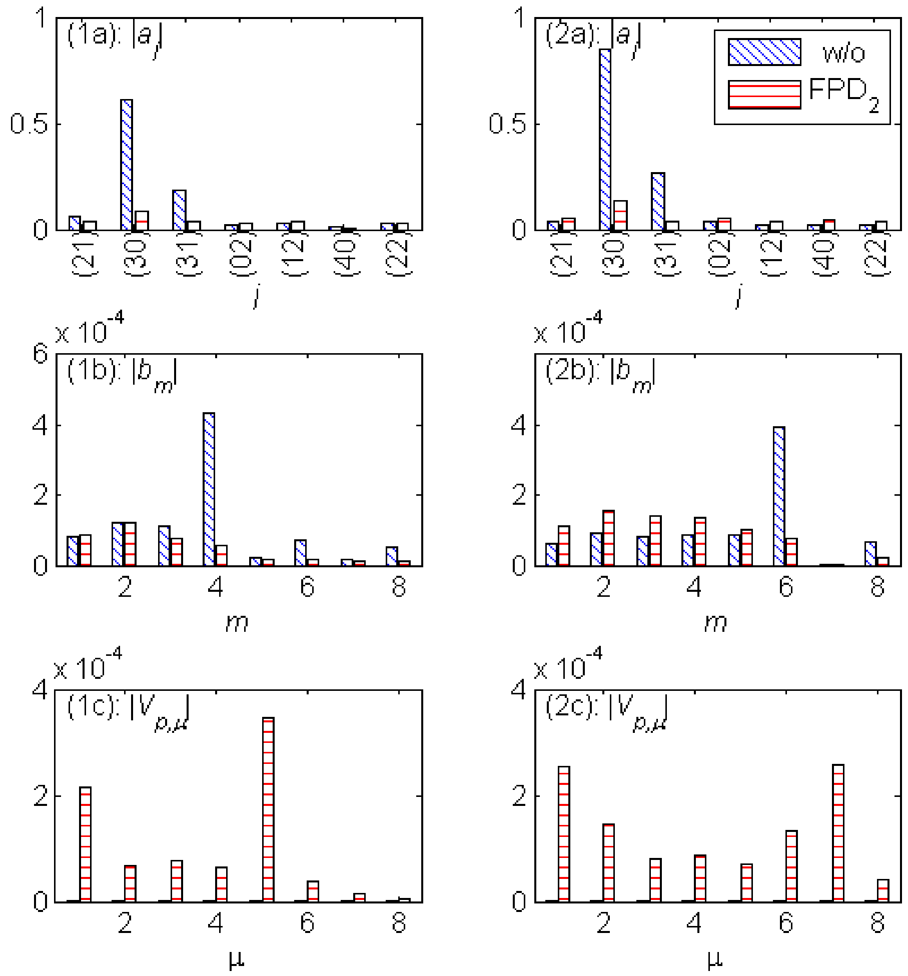

Fig. 6. Comparison of amplitudes of the enclosed cavity mode, external mode and panel vibration mode for the parallel barriers with and without FPD_2.

As shown in Fig. 6(1a) and (1b), the sound field inside the cavity space Ω_a is dominated by the cavity mode (3,0), while the sound response in the outside space Ω_b is dominated by the fourth external mode. At 289 Hz, the response of the cavity mode (3,0) is high. Consequently, a reverberant sound field is formed inside the cavity space when no acoustic treatment. When the FPD_2 is mounted, its panel vibrates dominantly in the first and fifth mode. The fifth modal response of the panel leads to an effectively radiating sound wave, which experiences acoustic interaction with the sound field inside the cavity space confined by the parallel barriers. In this situation, the cavity acoustic modal response at (3,0) is suppressed immensely, while the amplitudes of the other modes change slightly. Consequently, the sound field inside the cavity space at this frequency is reduced and less energy radiates out. As a result, the modal coefficient of the corresponding external mode is decreased, and the SPL at R1 is reduced. A similar performance can be observed at 474 Hz although the dominant modal indices are different. At 474 Hz, the dominant vibration responses of the panel are the first and seventh mode. The panel can still radiate sound. However, it is less effective than at 289 Hz because the sound radiation effectiveness is reduced at a higher modal response of the panel. Consequently, the noise reduction at that spectral peak is below that at 289 Hz. The modal response analysis indicates that the noise reduction is achieved by the effective vibration of FPD_2. The sound radiation from the vibrating panel undergoes acoustic interference with the sound waves inside the barrier space, thereby leading to a distortion of the sound field between the parallel barriers. In addition, the vibrating panel response is influenced by the sound field inside the backing cavity. Therefore, the SPL peak suppression strategy cannot be achieved by solely matching the resonance of the panel. Furthermore, distinguishing the resonant features of the panel and coupled panel is difficult. As a preliminary investigation, the root-mean-square result instead of the panel resonance is tactically used to explore the relationship between the noise reduction in the spectrum and resonances of the panel. The effect of the backing cavity on the plate vibration and hence the sound radiation suppression of the open acoustic system will be investigated in the future. The panel response can be expressed with the root-mean-square value:

$$V_{rms} = \left(\sum_{\mu} \left| V_{p,\mu} \right|^2 \Big/ 2 \right)^{1/2}, \tag{35}$$

where $V_{p,\mu}$ is the amplitude of the panel vibration mode defined in Eq.(17).

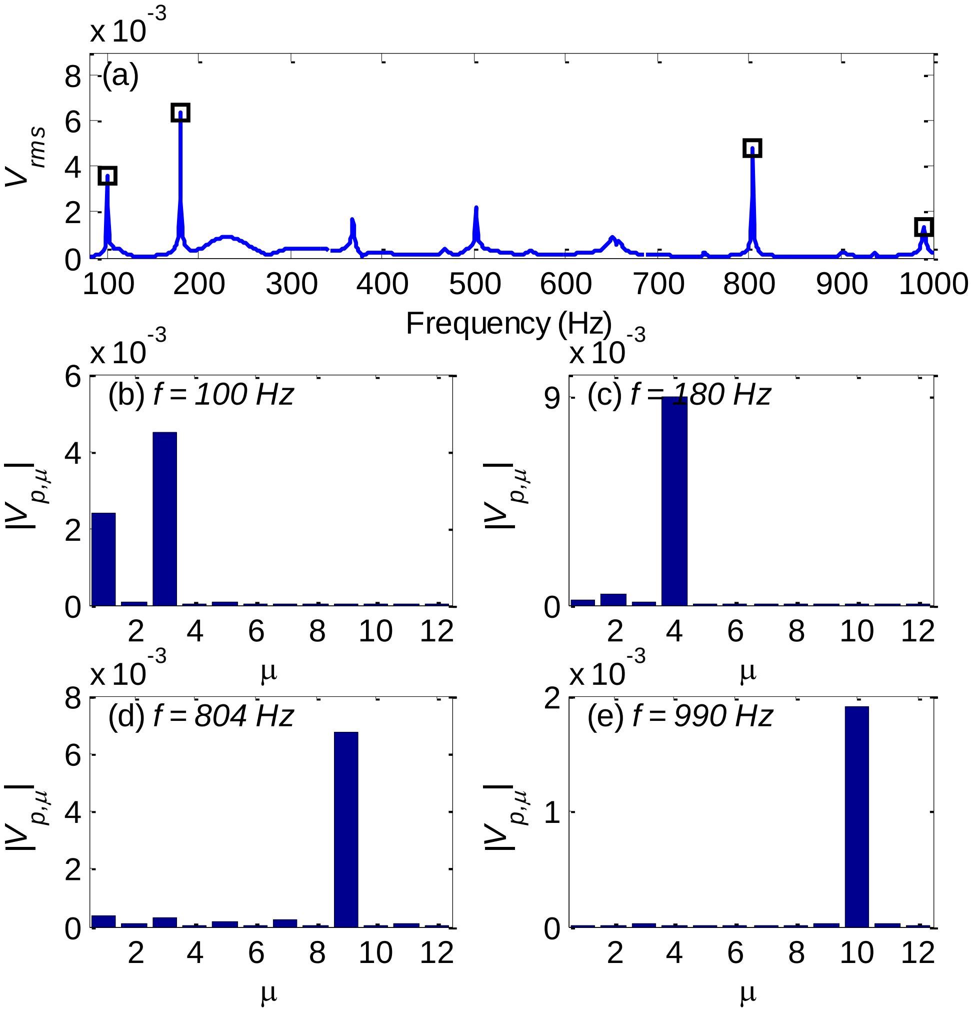

Fig. 7. Response of the panel of FPD2. (a) V_{rms}; (b), (c), (d) and (e) are the panel vibration modal components at 100, 180, 804 and 990 Hz respectively.

Fig. 7(a) shows the V_{rms} spectrum, and four of its peaks are marked with squares. The corresponding components of the modal responses at 100, 180, 804 and 990 Hz are shown in Fig. 7(b), 7(c), 7(d) and 7(e), respectively. The first V_{rms} peak at 100 Hz is dominated by the first and third modes (μ =1 and 3). At this frequency, there is a sound pressure antinode along the major part of the panel, and most of the sound is radiated effectively by the panel. As a result, the radiated sound wave and original sound field inside the cavity space experience a strong destructive interference, and SPL at R1 is suppressed. However, V_{rms} is high at 804 and 990 Hz and the corresponding modal responses of the panel are mainly contributed by the ninth and tenth modes. Nevertheless, the effectiveness of the sound radiation from the panel by these high-order modes is low, and the vibro-acoustic interaction is therefore too weak to achieve sound suppression inside and outside the cavity space.

3.3.2 Diffraction effect

The sound suppression capability of the FPD at the receiver point behind the barrier depends on the change in the sound diffraction at the top edge of the barrier wall. When the incident waves arrive at the barrier top, the sound field becomes a secondary source, which generates diffracting waves. The sound pressure at the receiving point in the shadow zone is determined by the sound pressure and diffraction coefficient at this diffraction point R_d [24, 25]. Moreover, the location of R_d for the right-hand shadow region can be seen in Fig. 1. With a fixed receiver, the diffraction coefficient is mainly determined by the angle of incident sound reaching R_d. Therefore, observing the changes in the sound level and incident angle at R_d can help to predict the SPL variation at the receiver.

Fig. 8(a) shows the SPL at R_d, while Fig. 8(1b) and 8(2b) present the sound intensity field at 381 Hz for the parallel barrier without and with FPD_2, respectively. According to Fig. 8(a), the SPL at the diffraction point R_d decreases at most peaks with FPD_2; this behavior is consist with that at R1. The peak reduction is attributed to the effective destructive sound interference among the radiated wave from the panel and the reflected wave from the remaining rigid walls and original sound. At the first SPL_d peak, V_{rms} in Fig. 7(a) and the first modal response of the panel are high. Thus, it can radiate the sound wave effectively. At the second SPL_d peak, V_{rms} is high. However, the dominant modal response of the panel is the fourth mode. Thus, the sound radiation effectiveness is relatively weak, and the sound reduction is not as high as that at the third and fourth peaks. At the third SPL_d peak, V_{rms} is low. Nevertheless, the dominant modal response at the first mode is high, and the sound radiation from the panel is sufficiently high for acoustic interactions with the sound waves inside the parallel barriers. However, Fig. 8(1b) shows that the incident sound wave normally reaches the diffraction point when the parallel barrier surfaces are acoustically rigid, and as a result, the diffraction coefficient is close to the maximum. When the FPD_2 is mounted on the surface of the parallel barriers, the incidence angle at the top edge of the wall is bent in direction parallel to the vertical wall as shown in Fig. 8(2b). This leads to a smaller diffraction coefficient. The reason is that the sound wave radiated from the panel travelling along the direction parallel to the left vertical wall bends the original incident sound wave with normal direction in direction parallel to the vertical wall. Thus, the diffracting wave bends more into the vertical direction. Because both sound pressure and diffraction coefficient are reduced at the top edge of the barrier, the noise reduction in the shadow zone behind the parallel barriers can be achieved. In summary, the panel works as a sound radiator that suppresses or increases the SPL at the diffraction point depending on the modal amplitudes and its radiation efficiency.

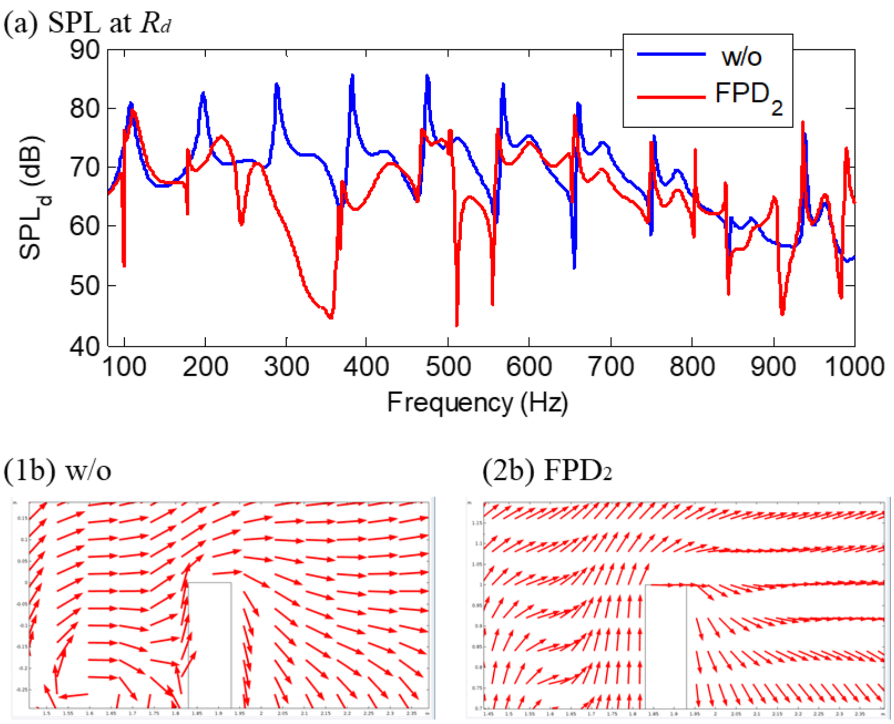

Fig. 8. SPL at the diffracting point R_d and the acoustic intensity around R_d. (a) SPL_d at R_d. (1b) and (2b) acoustic intensity at 381 Hz for parallel barriers without and with FPD_2, respectively.

4 Parametric studies of FPD

Although the FPD is a very simple device for constructions, it does have a lot of variables that substantially influence the noise abatement performance. These variables include geometrical variables such as the length, depth and location of the backing cavity and structural properties such as the bending stiffness and the mass. By considering the practical implementation, the cavity depth is 0.1 m, which is equal to the wall thickness of the barriers, and the lengths of the panel as well as the backing cavity are 0.4 m. The resonator results indicate that the working area of the device should not be far from the noise source [10, 35]. Moreover, the FPD is flush-mounted on the inner surface of the left side barrier at 0.1 m above the ground.

4.1 Effect of structural property of panel

The effect of the structural panel properties including its mass and bending stiffness are discussed in this section. Fig. 9-11 show the SPL spectra at receiving point R1 for different bending stiffnesses B_p when the panel mass is 0.2, 0.4 and 1 kg m^{-1}, respectively. Fig. 9 displays the results for m_p = 0.2 kg m^{-1}, and the value of B_p for each stacked spectrum are provided on the left-hand side. When the bending stiffness B_p increases, the resonant frequencies of the panel shift toward higher frequencies, and the SPL spectrum at R1 shifts slightly to higher frequencies. Roughly speaking, the SPL around most original sound peaks are reduced. However, the SPL between the separated peak frequencies are enhanced. For example, for B_p = 0.1 N m^{-1}, the SPLs at 289 and 381 Hz decrease from 69.9 and 71.3 dB to 51.3 and 53 dB, respectively. Thus, a noise reduction of over 18 dB is achieved at these two sound peaks. However, the SPL at 315 Hz increases from 58.4 to 70.4 dB. Hence, the average reduction with FPD is approximately -0.6 dB at 80 – 1000 Hz. When the panel mass is increased to 0.4 kg m^{-1}, more panel resonances appear at 180 – 750 Hz. As shown in Fig. 10, the SPL spectra are suppressed at the original sound peaks and the frequency ranges within and close to these peaks. Hence, broadband noise reduction can be achieved. Another advantage of increasing the panel mass from 0.2 to 0.4 kg m^{-1} is that the SPLs at 750 – 900 Hz increases barely. With further increasing panel mass to 1 kg m^{-1}, the noise reduction can only occur at few sound peaks, as displayed in Fig. 11. For instance, for B_p = 1 N m^{-1}, the sound is merely suppressed at frequencies near 199 Hz. At other frequencies, the sound reduction features narrow band. This is because the panel with high mass or very high bending stiffness is difficult to excite in vibrations. Consequently, the interaction between the sound radiation from the panel and sound field between the parallel barrier is weak. At most frequencies, the panel with a high mass (m_p = 1 kg m^{-1}) behaves as a rigid wall and has little influence on the sound field inside the barrier space.

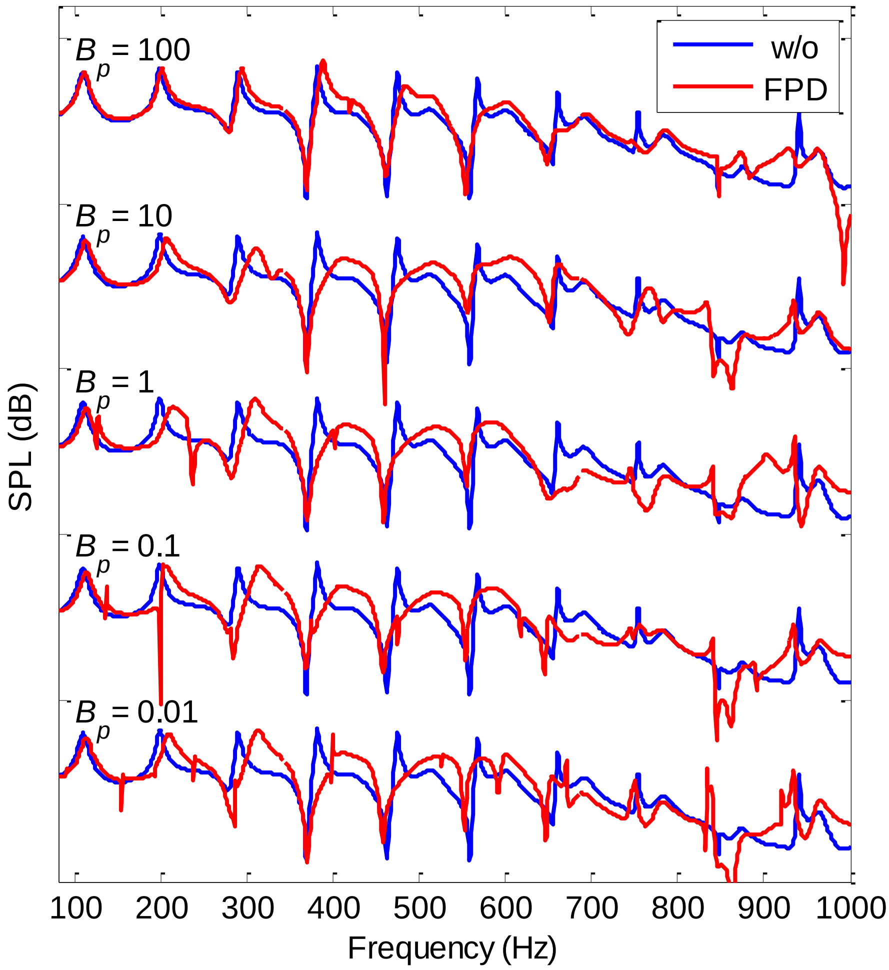

Fig. 9. SPL variation with panel bending stiffness at m_p = 0.2 kg m^{-1}.

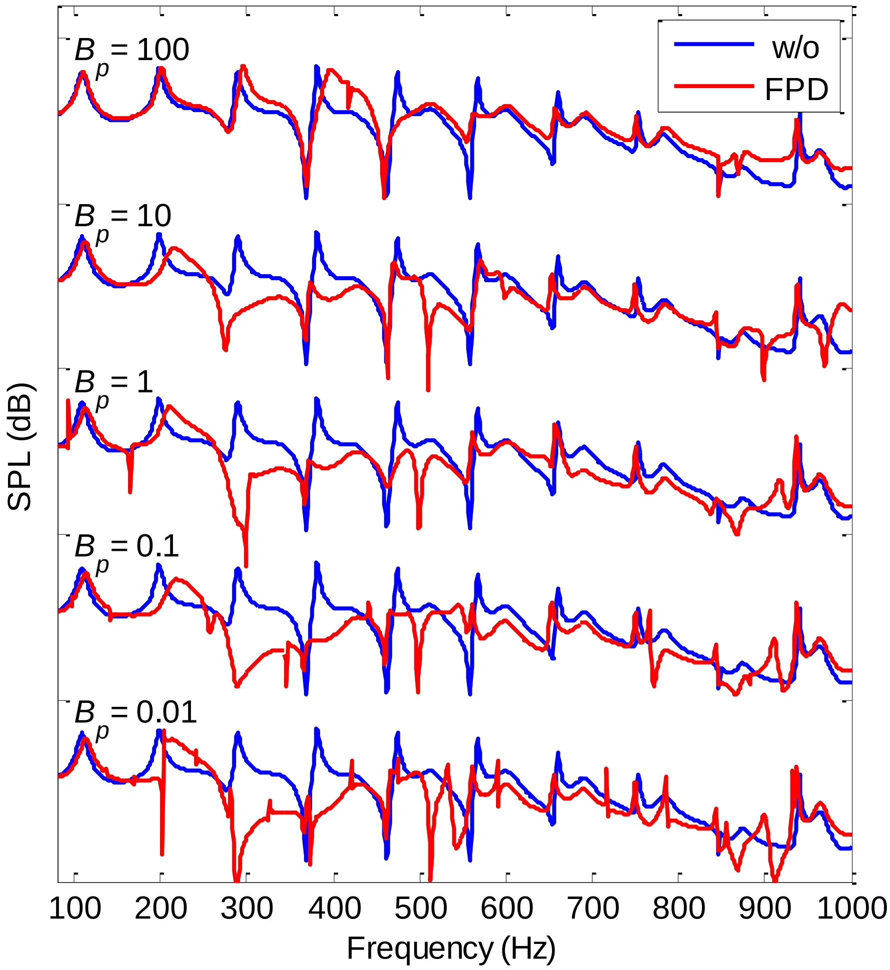

514

515 Fig. 10. SPL variation with panel bending stiffness at m_p = 0.4 kg m^{-1}.

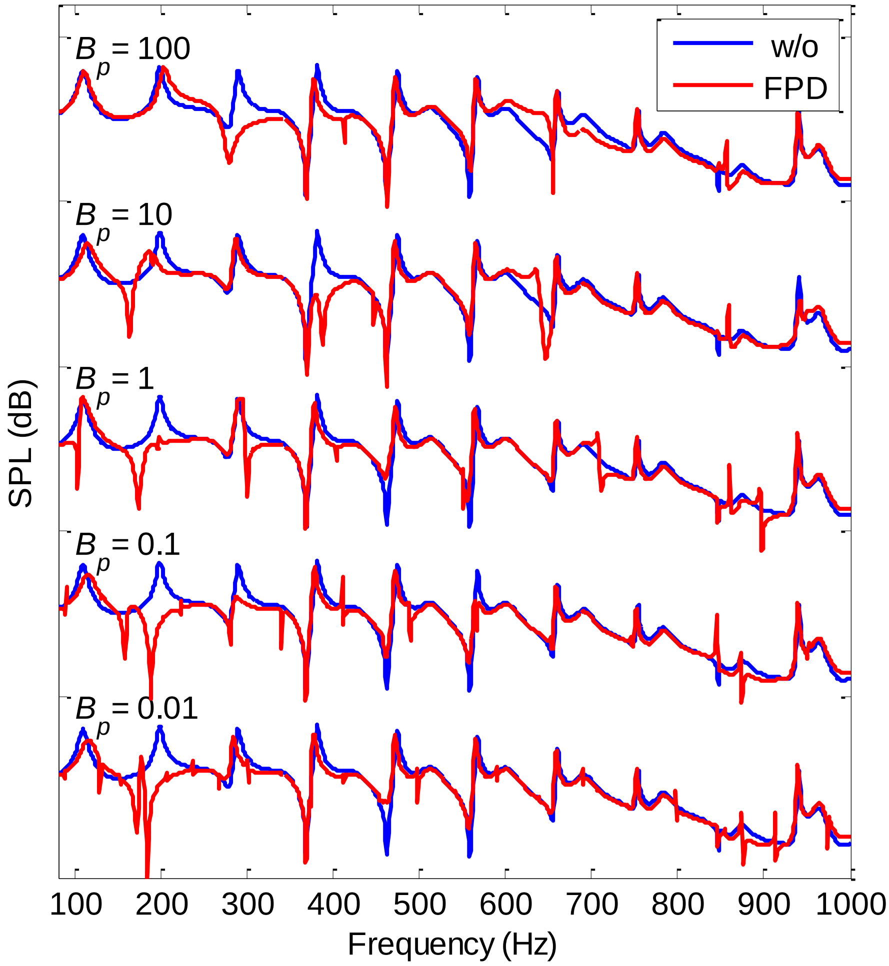

Fig. 11. SPL variation with panel bending stiffness at m_p = 1 kg m^{-1}.

4.2 Optimization of mass and bending

Fig. 9 – Fig. 11 demonstrate that with appropriate mass and bending stiffness, the SPL at the original peaks can be suppressed, and broadband noise reduction can be obtained. Hence, it is necessary to optimize the structural property of the panel to achieve the highest noise reduction in the low–frequency range. The mean insertion loss (IL_{mean}) within a target frequency range can be used to characterize the performance of the FPD:

$$IL_{mean} = \frac{\sum_{f_L}^{f_U} \left(SPL_{w/o}(f) - SPL_{FPD}(f) \right)}{N_f}, \tag{36}$$

where the subscripts "w/o" and "FPD" represent the parallel barriers without and with FPD, respectively; N_f is the total number of sampling frequencies used for calculating the SPL and $[f_L, f_U]$ is [80, 1000] Hz.

Fig. 12 indicates the variation in IL_{mean} at R1 when the FPD is installed at (0, -0.9) m with fixed geometrical parameters and variable panel bending and mass; IL_{mean} is negative when the panel is too light because, as indicated in Fig. 9, the original low SPL peak is slightly increased when the acoustically rigid wall is replaced with a light panel. When the panel mass is over 1.5 kg m^{-1}, the averaged insertion loss is approximately 1 dB. For the case of the panel bending stiffness is too high, approaching the acoustically rigid condition, the IL_{mean} is decreased. A good performance can be obtained for a panel mass of 0.25 – 0.7 kg m^{-1} and panel bending stiffness of approximately 0.01 – 3.6 N m^{-1}. With this mass and bending stiffness, the resonances of the FPD are close to the SPL peaks at R1 induced by the rigid parallel barriers. The destructive acoustic interference occurs among the sound radiation from the source, vibrating panel, and sound field between the barrier walls and ground**.** Furthermore, the original low SPL is slightly affected. Therefore, additional insertion loss can be achieved in the broad low–frequency band. The optimized structural parameters are m_p = 0.4 kg m^{-1} and B_p = 1.5 N m^{-1} and the highest average noise reduction at 80 – 1000 Hz is IL_{mean} = 3.95 dB.

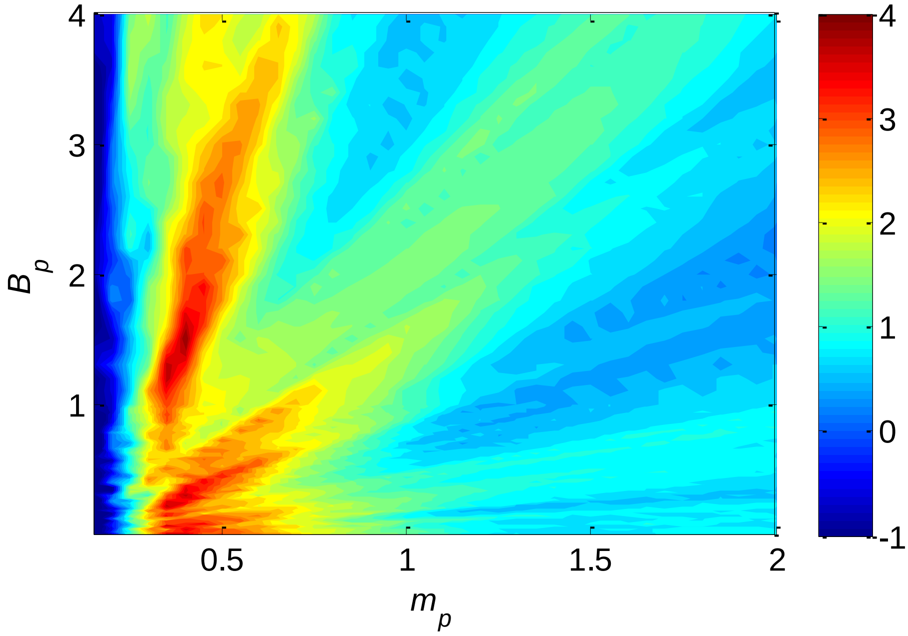

Fig. 12. IL_{mean} contour as a function of the panel mass and bending stiffness.

5 Experimental validation

The experimental study was conducted in the anechoic chamber. The barriers were 1 m in height and 4.8 m in length and were placed parallel to each other with a distance of 1.83 m. A speaker mounted on a long brass pipe with a length of l.5 m and diameter of 25 mm was used to simulate a point sound source. The point sound source was located 0.1 m away from one of the barriers and at a height of 0.1 m above the ground. One B&K 4189 microphone, connected to a B&K NEXUS conditional amplifier and a NI 9234 preamplifier, was employed to capture the acoustic signal. The location of the microphone was chosen at 1 m behind the barrier and a height of 0.2 m above the ground. The details about the experimental setup is shown in Fig. 13(a).

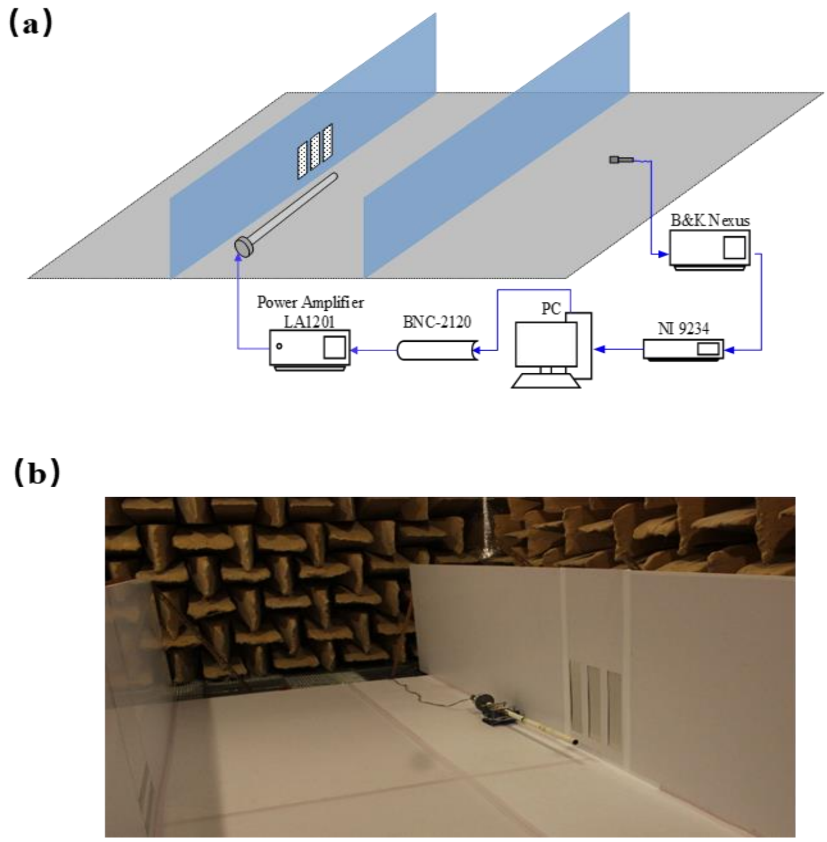

Fig. 13. Sound pressure measurement system. (a) Experimental set-up and (b) a photo of the parallel barriers in anechoic chamber.

The parallel barriers and ground surfaces were made of 18.5 mm thick wooden boards with varnishing [36], as indicated in Fig. 13(b). The PMI foam with density of 32 kg m^{-3} and Young's modulus of 0.036 Gpa was chosen as the flexible panel. The dimension of the panel is 420 mm in length, 104 mm in width and 2 mm in thickness. The panel was slightly larger than the backing cavity to prevent sound leakage through the panel edges. Two ends of the panel were clamped, and the other two lateral edges were inserted into a thin gap between two constituent plates of the cavity walls. There was a very small clearance (~1 mm) between the lateral edges of the panel and the backing cavity wall such that the lateral edges could freely vibrate to simulate the two-dimensional behavior.

Fig. 14 shows the measured SPL results for the parallel barriers with and without

FPD. The SPL at 384, 487 and 592 Hz are all reduced by at least 3 dB. Apart from the reduction at the sound peaks, the SPL in the frequency range of 351 Hz to 399 Hz is deceased by about 3.9 dB on average. Roughly speaking, the measured SPL results of the parallel barriers with and without the FPD match the predicted data derived from the theoretical model. The experimental results proved that the FPD can improve the noise reduction of the parallel barriers.

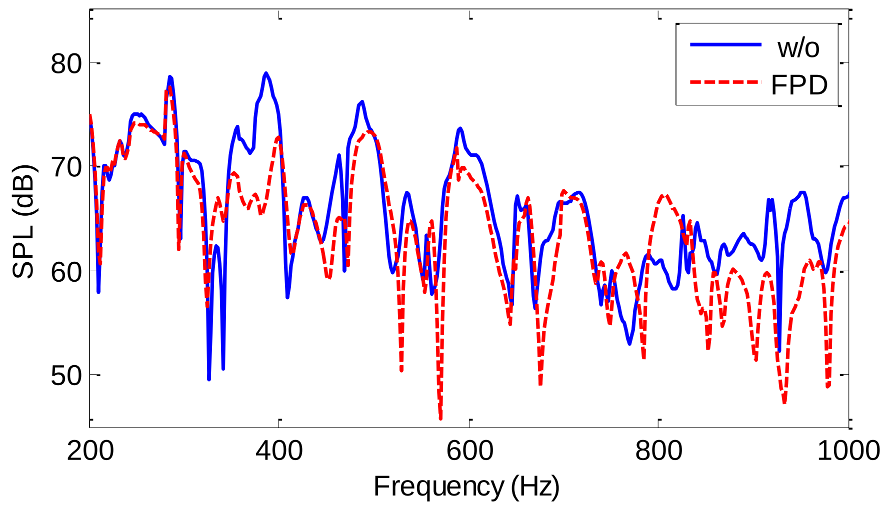

Fig. 14. Comparison of the measured SPL results for the parallel barriers with and without FPD.

6 Conclusions

The performance of a parallel barrier integrated with FPD via vibro-acoustic coupling was investigated theoretically and experimentally. The benefit provided by the vibrating panel to the parallel barriers is the suppression of the sound level for a wide frequency range, in particular the resonant frequencies of the open cavity system, through the interaction between the sound radiation from the vibrating panel and sound field inside the barrier space. The following specific conclusions can be drawn:

1. A theoretical model, capable of dealing with vibro-acoustic coupling between the vibrating panel and sound field of the parallel barriers was developed.

Characterizing the sound fields in the confined cavity and the semi-infinite spaces, the theoretical model can also be used as a systematical analysis, design and optimization tool for noise control of open cavity based on vibro-acoustic coupling. **A theoretical model which can deal with vibro-acoustic coupling between the vibrating panel and sound field inside and outside two-dimensional open cavities was developed. Because it also characterizes the sound field in the confined cavity and semi-infinite spaces, it can be used for systematical analyses and as design and optimization tool for noise control of parallel barriers based on vibro-acoustic coupling.**

2. With suitable panel properties, the sound radiation from the panel due to its vibration in response to the incident sound undergoes sound cancelation with the sound field within the barrier space. Consequently, the incident sound at the barrier top edge is suppressed, which reduces the diffraction wave that propagates from the top edge into the shadow zone. With optimized values for the flexible panel (m_p = 0.4 kg m^{-1}, B_p = 1.5 N m^{-1} and L_p = 0.4 m), the averaged noise reduction can exceed 3.95 dB at 80–1000 Hz. Moreover, the system can achieve a wider stopband than the Helmholtz resonator array.
3. The panel vibrations with moderately high amplitude and effective radiation efficiency promote the interaction between the sound radiated by the panel and the original sound field inside the parallel barriers. Moreover, the radiated sound wave that propagates along the vertical direction upward bends the original sound wave in direction parallel to the vertical wall. Hence, the sound level and the diffraction coefficient at the top edge of the parallel barriers is reduced, which reduces the SPL in the shadow zone behind the barriers.

4. An experimental study was conducted to verify the theoretical model and demonstrate the feasibility of the FPD in improving the noise reduction performance of parallel barriers. According to the results, the measured sound levels of the parallel barriers with and without FPD agree with the predicted data obtained with the theoretical model.

Acknowledgements

The authors would like to acknowledge the funding support from Innovation Technology Fund (UIM381) and The Hong Kong Polytechnic University (G-YBN2), (G-YBYA) and (G-YBL0).

Appendix-A

For vertical clamped-clamped beam, the mode shape function $\hbar_{\mu}$ at local coordinate ξ is governed by

$$\frac{d^4\hbar_{\mu}}{d\xi^4}-\gamma\frac{d}{d\xi}\left[\left(1-\xi\right)\frac{d\hbar_{\mu}}{d\xi}\right]-\frac{\Lambda}{i\omega}\hbar_{\mu}=0. \tag{A.1}$$

The boundary conditions at the two ends for the vertically clamped-clamped Euler-Bernoulli beam are

$$\hbar_{\mu}\left(0\right)=0,\qquad \frac{d}{d\xi}\hbar_{\mu}\left(0\right)=0, \tag{A.2}$$

$$\hbar_{\mu}\left(1\right)=0,\qquad \frac{d}{d\xi}\hbar_{\mu}\left(1\right)=0. \tag{A.3}$$

An approximate approach for achieving a dosed form analytical solution is performed using Galerkin's method with beam eigenfunctions ϑ_t (without gravity) as comparison functions in a Ritz expansion:

$$\hbar_{\mu}\left(\xi\right)=\sum_{t=1}^{T}c_t\vartheta_t\left(\xi\right), \tag{A.4}$$

where c_t are an undetermined coefficients, $\vartheta_t\left(\xi\right)$ are functions [37]

$$\vartheta_t\left(\xi\right)=\cosh\left(\lambda_t\xi\right)-\cos\left(\lambda_t\xi\right)-\sigma_t\left[\sinh\left(\lambda_t\xi\right)-\sin\left(\lambda_t\xi\right)\right], \tag{A.5}$$

with

$$\sigma_t=\frac{\cosh\left(\lambda_t\right)-\cos\left(\lambda_t\right)}{\sinh\left(\lambda_t\right)-\sin\left(\lambda_t\right)}, \quad \cos\left(\lambda_t\right)\cosh\left(\lambda_t\right)=1. \tag{A.6}$$

Applying the standard Galerkin procedure, Eq.(A.1) can be modified to

$$\sum_{t=1}^{T}c_t\lambda_t\delta_{ts}-\gamma\int_0^1\vartheta_s\frac{d}{d\xi}\left[\left(1-\xi\right)\left(\sum_{t=1}^{T}c_t\frac{d\vartheta_t}{d\xi}\right)\right]d\xi-\frac{\Lambda}{i\omega}\sum_{t=1}^{T}c_t\delta_{ts}=0. \tag{A.7}$$

Finally, the special eigenvalue problem can be obtained by rearranging above equation

$$\left(\boldsymbol{\Upsilon}-\frac{\Lambda}{i\omega}\mathbf{I}\right)\mathbf{c}=0, \tag{A.8}$$

in which

$$\mathbf{c}=\left\{c_1,c_2,\cdots,c_T\right\}^T, \tag{A.9}$$

$$\Upsilon_{ts}=\lambda_t\delta_{ts}+\gamma\int_0^1\left[\frac{d\vartheta_s}{d\xi}\left(1-\xi\right)\frac{d\vartheta_t}{d\xi}\right]d\xi; \quad \boldsymbol{\Upsilon}=\begin{bmatrix}\Upsilon_{11},\Upsilon_{21},\cdots,\Upsilon_{T1}\\ \Upsilon_{12},\Upsilon_{22},\cdots,\Upsilon_{T2}\\ \ddots\\ \Upsilon_{1T},\Upsilon_{2T},\cdots,\Upsilon_{TT}\end{bmatrix}, \tag{A.10}$$

$$\mathbf{I}=\begin{bmatrix}1,\ 0,\ \cdots,\ 0\\ 0,\ 1,\ \cdots,\ 0\\ \ddots\\ 0,\ 0,\ \cdots,\ 1\end{bmatrix}. \tag{A.11}$$

The vanishment of the $\det\left(\boldsymbol{\Upsilon}-\frac{\Lambda}{i\omega}\mathbf{I}\right)$ yields the special eigenvalues λ_{μ} and eigenvector **c**. Therefore, the mode shape $\hbar_\mu$ for vertically clamped-clamped beam can be solved.

Appendix-B

In Eqs. (32)-(34), the elements are expressed as

$$\mathbf{M} = -i\rho\omega\begin{Bmatrix} \dfrac{\psi_{1y}(0)\delta_{1x,1}}{\left(k^2-k_1^2\right)}, \dfrac{\psi_{1y}(0)\delta_{1x,2}}{\left(k^2-k_1^2\right)}, \cdots, \dfrac{\psi_{1y}(0)\delta_{1x,M}}{\left(k^2-k_1^2\right)} \\ \dfrac{\psi_{2y}(0)\delta_{2x,1}}{\left(k^2-k_2^2\right)}, \dfrac{\psi_{2y}(0)\delta_{2x,2}}{\left(k^2-k_2^2\right)}, \cdots, \dfrac{\psi_{2y}(0)\delta_{2x,M}}{\left(k^2-k_2^2\right)} \\ \vdots \\ \dfrac{\psi_{Ny}(0)\delta_{Nx,1}}{\left(k^2-k_N^2\right)}, \dfrac{\psi_{Ny}(0)\delta_{Nx,2}}{\left(k^2-k_N^2\right)}, \cdots, \dfrac{\psi_{Ny}(0)\delta_{Nx,M}}{\left(k^2-k_N^2\right)} \end{Bmatrix}, \tag{B.1}$$

$$\mathbf{H} = -i\rho\omega\begin{Bmatrix} \dfrac{h_{1,1}}{\left(k^2-k_1^2\right)}, \dfrac{h_{1,2}}{\left(k^2-k_1^2\right)}, \cdots, \dfrac{h_{1,U}}{\left(k^2-k_1^2\right)} \\ \dfrac{h_{2,1}}{\left(k^2-k_2^2\right)}, \dfrac{h_{2,2}}{\left(k^2-k_2^2\right)}, \cdots, \dfrac{h_{2,U}}{\left(k^2-k_2^2\right)} \\ \vdots \\ \dfrac{h_{N,1}}{\left(k^2-k_N^2\right)}, \dfrac{h_{N,2}}{\left(k^2-k_N^2\right)}, \cdots, \dfrac{h_{N,U}}{\left(k^2-k_N^2\right)} \end{Bmatrix}, \tag{B.2}$$

$$\mathbf{S} = -i\rho\omega q_s \left\{ \frac{\phi_1(\vec{x}_s)}{\left(k^2-k_1^2\right)}, \frac{\phi_2(\vec{x}_s)}{\left(k^2-k_2^2\right)}, \cdots, \frac{\phi_N(\vec{x}_s)}{\left(k^2-k_N^2\right)} \right\}^T, \tag{B.3}$$

$$\mathbf{\Phi} = \begin{bmatrix} \delta_{1x,1}\psi_{1y}(0), & \delta_{2x,1}\psi_{2y}(0), & \cdots, & \delta_{Nx,1}\psi_{Ny}(0) \\ \delta_{1x,2}\psi_{1y}(0), & \delta_{2x,2}\psi_{2y}(0), & \cdots, & \delta_{Nx,2}\psi_{Ny}(0) \\ & \vdots & & \\ \delta_{1x,NX}\psi_{1y}(0), & \delta_{2x,NX}\psi_{2y}(0), & \cdots, & \delta_{Nx,NX}\psi_{Ny}(0) \end{bmatrix}, \tag{B.4}$$

$$Z_{\mu,m} = \int_s \int_s \left[\psi_\mu (x') \cdot \varphi_m (x) \right] ds ds'$$
$$\mathbf{Z} = \frac{1}{2} \rho \omega \begin{bmatrix} Z_{1,1}, & Z_{1,2}, & \cdots, & Z_{1,M} \\ Z_{2,1}, & Z_{2,2}, & \cdots, & Z_{2,M} \\ & \vdots & & \\ Z_{NX,1}, & Z_{NX,2}, & \cdots, & Z_{NX,M} \end{bmatrix}, \tag{B.5}$$

$$L_\mu = \frac{B_p}{i\omega} \left(\frac{\lambda_\mu}{L_p} \right)^4 + m_p i\omega;$$
$$\mathbf{L} = \left\{ \begin{matrix} L_1, & 0, & \cdots & , 0 \\ 0, & L_2, & \cdots & , 0 \\ \vdots & & & \\ 0, & 0, & \cdots & , L_U \end{matrix} \right\}, \tag{B.6}$$

$$Z_{cav,i\mu} = \int_0^1 \hbar_i (\xi) \, p_{cav,\mu} (\xi) \, d\xi$$
$$\mathbf{Z_{cav}} = \left\{ \begin{matrix} Z_{cav,11}, & Z_{cav,12}, & \cdots, & Z_{cav,1U} \\ Z_{cav,21}, & Z_{cav,22}, & \cdots, & Z_{cav,2U} \\ \vdots & & & \\ Z_{cav,U1}, & Z_{cav,U2}, & \cdots, & Z_{cav,UU} \end{matrix} \right\}, \tag{B.7}$$

$$Z_{a,\mu j} = \int_0^1 \hbar_\mu (\xi) \phi_j (\xi) \, d\xi$$
$$\mathbf{Z_a} = \begin{bmatrix} Z_{enl,11}, Z_{enl,12}, \cdots, Z_{enl,1N} \\ Z_{enl,21}, Z_{enl,22}, \cdots, Z_{enl,2N} \\ \vdots \\ Z_{enl,U1}, Z_{enl,U2}, \cdots, Z_{enl,UN} \end{bmatrix}. \tag{B.8}$$

References

[1] D. Hutchins, H. Jones, B. Paterson, L. Russell, Studies of parallel barrier performance by acoustical modeling, J. Acoust. Soc. Am. 77 (1985) 536-546.

[2] C. Yang, J. Pan, L. Cheng, A mechanism study of sound wave-trapping barriers, J. Acoust. Soc. Am. 134 (2013) 1960-1969.

[3] G. Watts, Acoustic performance of parallel traffic noise barriers, Appl. Acoust. 47 (1996) 95-119.

[4] T. Ishizuka, K. Fujiwara, Performance of noise barriers with various edge shapes and acoustical conditions, Appl. Acoust. 65 (2004) 125-141.

[5] D. Crombie, D. Hothersall, The performance of multiple noise barriers, J. Sound Vib. 176 (1994) 459-473.

[6] D.N. May, N. Osman, Highway noise barriers: new shapes, J. Sound Vib. 71 (1980) 73-101.

[7] M.R. Monazzam, S.M.B. Fard, Impacts of different median barrier shapes on a roadside environmental noise screen, Environ. Eng. Sci. 28 (2011) 435-441.

[8] J. Pan, R. Ming, J. Guo, Wave trapping barriers, in: Proceedings of acoustics, 2004. Gold Coast, Australia.

[9] X. Wang, D. Mao, W. Yu, Z. Jiang, Sound barriers from materials of inhomogeneous impedance, J. Acoust. Soc. Am. 137 (2015) 3190-3197.

[10] Z.B. Wang, Y.S. Choy, Tunable parallel barriers using Helmholtz resonator, J. Sound Vib. 443 (2019) 109-123.

[11] L. Huang, Broadband sound reflection by plates covering side-branch cavities in a duct, J. Acoust. Soc. Am. 119 (2006) 2628-2638.

[12] C. Wang, J. Han, L. Huang, Optimization of a clamped plate silencer, J. Acoust. Soc. Am. 121 (2007) 949-960.

[13] C. Wang, L. Huang, Time-domain simulation of acoustic wave propagation and interaction with flexible structures using Chebyshev collocation method, J. Sound Vib. 331 (2012) 4343-4358.

[14] X. Wang, Y. Choy, L. Cheng, Hybrid noise control in a duct using a light micro-perforated plate, J. Acoust. Soc. Am. 132 (2012) 3778-3787.

[15] Q. Xi, Y. Choy, L. Cheng, S. Tang, Noise control of dipole source by using micro-perforated panel housing, J. Sound Vib. 362 (2016) 39-55.

[16] E. Dowell, H. Voss, The effect of a cavity on panel vibration, AIAA. J. 1 (1963) 476-477.

[17] A. Pretlove, Free vibrations of a rectangular panel backed by a closed rectangular cavity by a closed rectangular cavity, J. Sound Vib. 2 (1965) 197-209.

[18] R. Guy, The steady state transmission of sound at normal and oblique incidence through a thin panel backed by a rectangular room–A multi-modal analysis, Acta Acust. United Acust. 43 (1979) 295-304.

[19] J. Pan, D.A. Bies, The effect of fluid–structural coupling on sound waves in an enclosure—theoretical part, J. Acoust. Soc. Am. 87 (1990) 691-707.

[20] N. Tanaka, Y. Takara, H. Iwamoto, Eigenpairs of a coupled rectangular cavity and its fundamental properties, J. Acoust. Soc. Am. 131 (2012) 1910-1921.

[21] Y.-H. Kim, S.-M. Kim, Solution of coupled acoustic problems: a partially opened cavity coupled with a membrane and a semi-infinite exterior field, J. Sound Vib. 254 (2002) 231-244.

[22] G. Jin, S. Shi, Z. Liu, Acoustic modeling of a three-dimensional rectangular opened enclosure coupled with a semi-infinite exterior field at the baffled opening, J. Acoust. Soc. Am. 140 (2016) 3675-3690.

[23] S. Shi, Z. Su, G. Jin, Z. Liu, Vibro-acoustic modeling and analysis of a coupled acoustic system comprising a partially opened cavity coupled with a flexible plate, Mech. Syst. Sig. Process. 98 (2018) 324-343.

[24] J.B. Keller, Geometrical theory of diffraction, J. Opt. Soc. Am. 52 (1962) 116-130.

[25] A.D. Pierce, Diffraction of sound around corners and over wide barriers, J. Acoust. Soc. Am. 55 (1974) 941-955.

[26] R. Seznec, Diffraction of sound around barriers: use of the boundary elements technique, J. Sound Vib. 73 (1980) 195-209.

[27] L. De Lacerda, L. Wrobel, H. Power, W. Mansur, A novel boundary integral formulation for three-dimensional analysis of thin acoustic barriers over an impedance plane, J. Acoust. Soc. Am. 104 (1998) 671-678.

[28] J.D.R. Bordón, J.J. Aznárez, O. Maeso, A 2D BEM–FEM approach for time harmonic fluid–structure interaction analysis of thin elastic bodies, Eng. Anal. Bound. Elem. 43 (2014) 19-29.

[29] F.-M. Dittes, The decay of quantum systems with a small number of open channels, Phys. Rep. 339 (2000) 215-316.

[30] K. Pichugin, H. Schanz, P. Šeba, Effective coupling for open billiards, Phys. Rev. E. 64 (2001) 056227.

[31] A. Lyapina, D. Maksimov, A. Pilipchuk, A. Sadreev, Bound states in the continuum in open acoustic resonators, J. Fluid Mech. 780 (2015) 370-387.

[32] Y. Tong, Y. Kou, J. Pan, Forced acoustical response of a cavity coupled with a semi-infinite space using coupled mode theory, Wave Motion. (2017).

[33] S. Naguleswaran, Vibration of a vertical cantilever with and without axial freedom at clamped end, J. Sound Vib. 146 (1991) 191-198.

[34] H. Kuttruff, Room acoustics, fifth ed., CRC Press, New York, 2009.

[35] Z. Wang, Y. Choy, Acoustical coupling and radiation control of open cavity using an array of Helmholtz resonators, Mech. Syst. Sig. Process. 130 (2019) 632-648.

[36] K. Li, M. Law, M. Kwok, Absorbent parallel noise barriers in urban environments, J. Sound Vib. 315 (2008) 239-257.

[37] D.J. Inman, Engineering vibration, fourth ed., Prentice Hall, New Jersey, 2008.

742